IEEE Access
Multidisciplinary | Rapid Review | Open Access Journal

Received 6 August 2023, accepted 14 August 2023, date of publication 15 August 2023, date of current version 22 August 2023.

Digital Object Identifier 10.1109/ACCESS.2023.3305680

RESEARCH ARTICLE

Display Visibility Improvement Through Content and Ambient Light-Adaptive Image Enhancement

JUNMIN LEE[1], HEEJIN LEE[1], SEUNGHYUN LEE[1], (Associate Member, IEEE), JUNHO HEO[2], JIWON LEE[2], AND BYUNG CHEOL SONG[1], (Senior Member, IEEE)

[1]Department of Electrical and Computer Engineering, Inha University, Incheon 22212, Republic of Korea
[2]LX Semicon, Daejeon 324027, Republic of Korea

Corresponding author: Byung Cheol Song (bcsong@inha.ac.kr)

This work was supported in part by the National Research Foundation of Korea (NRF) Grant funded by the Korea Government [Ministry of Science and ICT (MSIT)] under Grant 2022R1A2C2010095 and Grant 2022R1A4A1033549, and in part by the Institute of Information and Communications Technology Planning and Evaluation (IITP) Grant funded by the Korea Government (MSIT) (Artificial Intelligence Convergence Innovation Human Resources Development (Inha University) and the Development of High-Definition CIS and High-Speed DVS Enabled AI SoC for Object and Motion Recognition) under Grant RS-2022-00155915 and Grant 2022-0-00955.

ABSTRACT An image in a display device under strong illuminance can be perceived as darker than the original due to the nature of the human visual system (HVS). In order to alleviate this degradation in terms of software, existing schemes employ global luminance compensation or tone mapping. However, since such approaches focus on restoring luminance only, it has a fundamental drawback that chrominance cannot be sufficiently restored. Also, the previous approaches seldom provide acceptable visibility because it does not consider the content of an input image. Furthermore, because they focus mainly on global image quality, they may show unsatisfactory image quality for certain local areas. This paper introduces VisibilityNet, a neural network model designed to restore both chrominance and luminance. By leveraging VisibilityNet, we generate an optimally enhanced dataset tailored to the ambient light conditions. Furthermore, employing the generated dataset and a convolutional neural network (CNN), we estimate weighted piece-wise linear enhancement curves (WPLECs) that take into account both ambient light and image content. These WPLECs effectively enhance global contrast by addressing both luminance and chrominance aspects. Ultimately, through the utilization of a salient object detection algorithm that emulates the HVS, visibility enhancement is achieved not only for the overall region but also for visually salient areas. We verified the performance of the proposed method by comparing it with five existing approaches in terms of two quantitative metrics for a dataset we built ourselves. Experimental findings substantiate that the proposed method surpasses alternative approaches by significantly improving visibility.

INDEX TERMS Visibility improvement, ambient light, piece-wise linear curve, salient object enhancement.

I. INTRODUCTION

Thanks to the help of semiconductor technology, mobile display devices with ultra-high resolution have made rapid progress. Furthermore, advancements in deep learning models like Convolutional Neural Networks (CNNs) have led to the development of many technologies that outperform traditional image quality enhancement algorithms [1], [2], [3]. As a result, we can now easily enjoy high-resolution videos anytime and anywhere. However, many display devices are still vulnerable to changes in ambient light. For example, when the ambient light is stronger than the display brightness as in an outdoor environment, the human visual system (HVS) suffers from a phenomenon that perceives an image on the display device to be darker than the original (Fig. 1). This degradation becomes more severe as the brightness gap between the display and the ambient light increases, which means a decrease in visibility on the display

The associate editor coordinating the review of this manuscript and approving it for publication was Sudhakar Radhakrishnan.

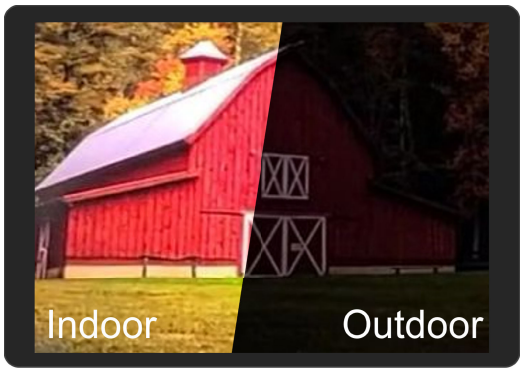

FIGURE 1. Visibility comparison under a light box set to indoors and outdoors.

device. Therefore, a new image enhancement algorithm is required to minimize visibility degradation due to the ambient light.

To solve this problem, a hardware-based approach [4] was presented where the display's brightness can be augmented by modulating the current of the back-light unit (BLU) in response to the measured illuminance. However, in outdoor settings, it is inevitable to fully eliminate the influence of ambient light, as noted by Kim et al. [5]. Additionally, the current hardware-based approach falls short of attaining satisfactory visibility. To overcome these limitations, alternative algorithmic approaches can be explored. As a rather trivial one, there are general contrast-enhancement techniques. For instance, we can increase visibility by using contrast-enhancement such as histogram equalization [6], [7] and multi-exposure image fusion [8], [9], [10]. The contrast of images can be enhanced through general image enhancement techniques [11], [12], [13] to improve images taken in diverse challenging environments (e.g., uneven illumination, complex underexposure, etc). In addition, there are low-light image enhancement techniques that aim to enhance the contrast of only images taken in low illumination environments [14], [15], [16], [17]. However, general contrast-enhancement techniques and low-light image enhancement techniques never consider degradation due to ambient light. That is, they have a disadvantage in that they cannot adjust image quality according to ambient light. Note that our goal is not to improve images captured in a diverse environment, but to improve images to look as similar as possible to the source image in a situation where the displayed image is degraded by ambient light. A more advanced approach can be ambient-light-adaptive image enhancement. But it focuses only on the luminance component, so it may suffer from color distortion [18], or it does not sufficiently improve the chrominance component(s). In addition, since the previous approach concentrates on global compensation only, it can face a decrease in local contrast [19]. We already proposed a solution [19] to resolve the limitations of previous works. In [19], we utilized deep learning techniques to generate pseudo-ground-truths (GTs). These GTs consist of images that have been adaptively enhanced to match the ambient light conditions. Drawing upon the generated dataset, the authors introduced piece-wise linear enhancement curves (PLECs) to improve global contrast, and further employed local contrast enhancement (LCE) techniques to enhance local contrast. However, the pseudo-GT method proposed by Lee et al. [19] fell short of effectively enhancing chrominance. Furthermore, both the PLECs and the LCE approaches have a drawback in that they do not take into account image content or the characteristics of the HVS.

This paper proposes the following solutions to overcome the limitations of our prior work [19]. First, we propose VisibilityNet to learn even chrominance components. VisibilityNet is trained in two steps: Step 1 enhances luminance components, and Step 2 trains the chrominance components by using the enhanced luminance components. Second, we propose weighted piece-wise linear enhancement curves (WPLECs). CNN extracts image content and then regress WPLECs taking the image content into account. Third, we propose salient object enhancement (SOE) which further improves the visibility of the main area by introducing a specific salient object detection (SOD) technique [20]. Therefore, the proposed method can effectively improve both luminance and chrominance in a content-adaptive fashion. Experiment results show that the proposed method provides qualitatively better visibility than previous methods under several ambient light settings, and they also provide a mean opinion score (MOS) as high as 0.59.

The contributions of the proposed method are summarized as follows:

- Using deep learning, we generated a dataset adaptive to ambient light without reference images.
- We introduced, for the first time, a CNN approach that enhances global contrast while considering the content of the image.
- We introduced SOD to achieve better visibility considering human perception under ambient light.

This paper is organized as follows: Section II introduces general contrast-enhancement techniques, low-light image enhancement techniques, and the conventional ambient-light-adaptive algorithm. Section III describes the proposed method: Section III-A explains our prior work in detail, Section III-B depicts the ambient-light-adaptive pseudo-GT generation with VisibilityNet, Section III-C describes content-aware global contrast-enhancement using the pseudo-GT, and Section III-D describes SOE to improve visibility of the main object(s). Section IV presents the qualitative evaluation results. Section V reports an ablation study of each step of the proposed method. Section VI deals with matters to be discussed later in our task and Section VII gives concluding remarks.

II. RELATED WORKS

A. GENERAL CONTRAST-ENHANCEMENT

The most basic solution to improve visibility may be general contrast-enhancement. For example, CLAHE [6] divides an

image into patches and applies histogram equalization on a patch basis; the logarithmic model [21] properly adjusts the image histogram through gamma correction; and SEF [8], [22] fuses multi-exposure images. Ye et al. [23] proposed LFIENet based on unsupervised learning. LFIENet enhances images by fusing the 4D light field (LF)-DSLR pair images. However, these algorithms have an inherent disadvantage in that they are not adaptive to ambient light.

B. LOW-LIGHT IMAGE ENHANCEMENT

The next thing to consider is low-light image enhancement (LLIE), which targets only for low-light images. For example, Li et al. [24] proposed progress-recursive network to enhance both global and local features. Ren et al. [25] enhanced low-light images with using the response characteristics of cameras. Guo et al. [17] proposed a lightweight DCE-Net which estimates pixel-wise and high order curves for low-light image enhancement. Xu et al. [26] applied STANet to preserve structure and texture features of enhanced image. Ma et al. [27] proposed an unsupervised learning model based on a cascaded learning process, and generated images with vivid color and sharp outline. Xu et al. [28] generated images with noise effectively removed through a model to which a signal-to-noise-ratio (SNR)-aware transformer and self-attention module were applied. Yang et al. [29] proposed a lightingNet consisting of a sub-network and ViT [30] to enhance local high level features and generate global fine-tuned features. Wang et al. [31] employed multi-scale modules to extract local and global features. And they effectively exploited angular correlation through 3D multi-scale modules based on extracted local and global information. Note that these algorithms aim to enhance the contrast of images taken in low light conditions. On the other hand, our task, i.e., visibility improvement, aims to improve images that are perceived as dark due to ambient light to look similar to the source images. Therefore, LLIEs are inevitably different from our task in terms of not only purpose but also approach. It is expected that the LLIE techniques can improve the visibility deteriorated by ambient light to some extent by enhancing the contrast of low-light images. However, LLIE does not consider the ambient light at all, so it is not adaptive to this. Furthermore, it may rather cause unwanted enhancement in a bright area other than the target.

C. AMBIENT-LIGHT-ADAPTIVE IMAGE ENHANCEMENT

To overcome the shortcomings in contrast-enhancement and LLIE, a few ambient-light-adaptive techniques have been proposed. Kim et al. [5] enhanced global luminance based on a light-adaptation model and compensated for chrominance according to ambient light. Mantiuk et al. [32] proposed piece-wise linear curve-based luminance compensation using a display adaptive tone mapping operation (DATMO), and performed chrominace compensation through a desaturated color-to-luminance ratio [33]. Wang and Jung [34] applied low-level enhancement using the Bartleson-Breneman equation [35] prior to tone mapping. Su et al. [36] succeeded in formulating constraint optimization to find the best trade-off from among luminance enhancement, contrast-enhancement, and distortion minimization. However, Kim et al.'s method [5] has a color cast problem [18]. Also, Mantiuk et al. [32], Wang and Jung [34], and Su et al. [36] simply defined the luminance enhancement level as a ratio and then compensated for the chrominance components by applying that ratio to the color channel as is, so performance is bound to be limited [19]. In summary, the above techniques made less of an effort to improve chrominance compared to improving luminance, and the disadvantage is not sufficiently improving color information. Furthermore, since they only perform global compensation, their approaches can lose local details during the process.

III. PROPOSED METHOD

A. PRIOR WORK

Before explaining the proposed method, we briefly introduce our prior work [19], which consists of a global contrast enhancement (GCE) step and a local contrast enhancement (LCE) step. GCE learns piece-wise linear enhancement curves (PLECs) using pseudo-GTs from pseudo-GT generation (PGG). Here, to achieve better visibility, PLECs for luminance and chrominance are regressed together. LCE detects a local area where the contrast is somewhat reduced due to GCE, and enhances the contrast of the local area.

1) PSEUDO-GT GENERATION

Any public dataset considering ambient light is not available yet. So, we generated a dataset according to ambient light by ourselves. Since reference images for generating pseudo-GTs do not exist, we used a degradation model, $\mathcal{D}$ [37], that simulates a phenomenon in which visibility of displayed images deteriorates due to the ambient light. $\mathcal{D}$ is calculated for the purpose of simultaneously reducing the perceptible contrast range and the noticeable grayscale differences. For a detailed description of this, please refer to Section 3.3.1 of Bauer et al.'s [37]. Based on $\mathcal{D}$, we generated a new dataset considering ambient light without reference images. The luminance component (Y channel) of the pseudo-GT was obtained by a neural network model called VENet. VENet was trained to minimize the difference betweenluminance Y_S of source image I_S and the $\mathcal{D}(Y_P)$ applied with $\mathcal{D}$ to the enhanced luminance, Y_P. To restore the chrominance information lost due to ambient light, we defined Eq. (1) by modifying the CbCr fusion formula [38], which creates the color of the image that is fused to the under-exposed and over-exposed images. We apply this concept to our task. After designating the under/over-exposed images as the degraded image and the original image, respectively, in the existing formula, an improved image is derived by calculating the inverse function. Eq. (1) is as follows. Here, C_P denotes the enhanced chrominance component:

$$C_P = C_{I_S}\left(1 - \frac{(C_{\mathcal{D}(I_S)}/C_S - 1)|C_{\mathcal{D}(I_S)} - \tau|}{2|C_S - \tau| - |C_{\mathcal{D}(I_S)} - \tau|}\right), \quad (1)$$

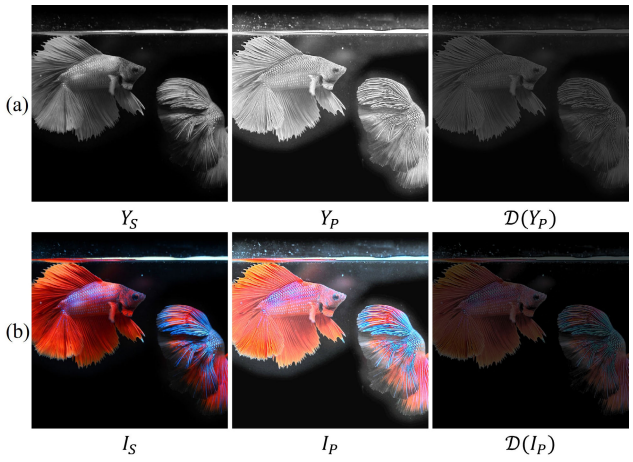

FIGURE 2. The pseudo-GT from our prior work: (a) shows the Y components of source image Y_S and result image Y_P enhanced by VENet, and (b) shows the source image I_S and result image I_P after concatenating Y_P with chrominance enhanced by Eq. (1). Here, the ambient light of $\mathcal{D}$ was set to 10,000lux.

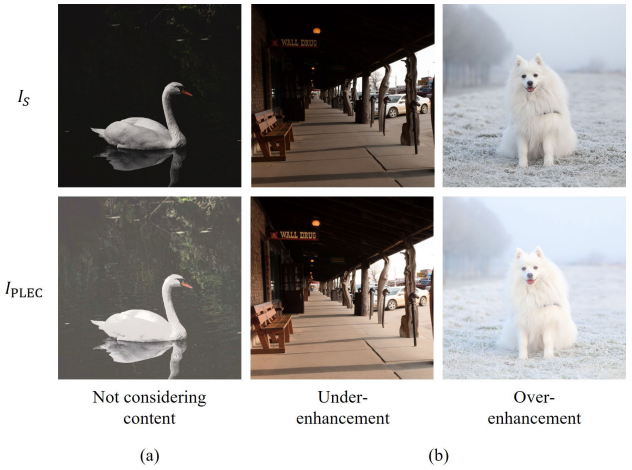

FIGURE 3. Limitations of the previous GCE. (a) Since only average brightness is considered, the bright area (e.g., the swan) in the image is not taken into account. (b) With under-enhancement, the low gray scale region needs to be further enhanced, and with over-enhancement, details of the dog's fur or grass disappear.

FIGURE 4. (a) is the input of LCE, (b) is the output of LCE (final output of prior work), and (c) is the weight map of LCE. (c) only detects the background, not the salient object. Also, looking at (b) through (c), the contrast of the horse, which is a salient object, is lowered, and background noise is amplified. As a result, overall visibility decreased.

where τ was set to 128. First, the chrominance $C_{\mathcal{D}(I_S)}$ with $\mathcal{D}$ applied to I_S and the chrominance C_S of the I_S, which have reduced expressible contrast due to the deterioration model with the characteristics of under-exposed and fused images, respectively, are set as inputs. Then, using the above modified formula, a color with improved contrast is obtained within a limited range.

Note that the PGG from [19] did not consider the correlation between chrominance and luminance. Fig. 2 demonstrates the limitation. First, we observe that Y_P preserves the entire information from Y_S while greatly enhancing the luminance component. In $\mathcal{D}(Y_P)$, the luminance is appropriately enhanced according to the ambient light. On the other hand, in I_P and $\mathcal{D}(I_P)$, a sort of wash-out phenomenon is observed. Thus, we require a novel solution beyond PGG from [19] which can enhance even chrominance reliably.

2) GLOBAL CONTRAST ENHANCEMENT

GCE enhances the global contrast of an image by using PLECs trained with pseudo-GTs. PLECs are mapping curves that play a role similar to gamma correction. In this paper, they are discretely implemented with seven control points that equally divide the range of each channel into eight sections. According to our experiment, if there are too many control points (e.g., 16 or more), the fitting tends to fail during learning. That is, it shows high variance. Also, if the number of control points is too small (e.g., 4 or less), it was rather difficult to perform proper color correction. That is, the bias increases. Based on these experimental results, we set the number of control points to eight. Here, the slope (a_i) of each section is learned so the PLECs-applied image I_{PLEC} is close to the pseudo-GT. Also, for monotonicity of PLECs, a ReLU is added so that a_i is always positive. Trained slope vectors A can be expressed by Eq. (2).

$$A_j = \text{ReLU}([a_1, a_2, \ldots, a_8]), \quad j \in \{S, V\} \tag{2}$$

In order to prevent color distortion and enhance both luminance and chrominance, PLECs are learned considering the correlations between saturation (S) and value (V) channels of HSV color format. So, two curves exist for each channel. Meanwhile, since the degree of degradation is affected by the image brightness, we regress the PLECs for three classes (dark, medium, bright). The class of an image is determined by the average brightness of the image.

However, this GCE has the following drawback. In general, scenes in the wild can be represented with various features such as context, object, and brightness distribution. So, if an image is classified by only one scalar, e.g., average brightness, various other features of the image cannot be reflected, as seen in Fig. 3 (a). In addition, hard classification causes a problem where images near the decision boundary of the classifier may be under- or over-enhanced (see Fig. 3 (b)). Therefore, we need to regress the PLECs optimized for each image while considering the image content.

3) LOCAL CONTRAST ENHANCEMENT

LCE adjusts pixels where the contrast deteriorates due to GCE. First, candidate pixels are detected on a patch basis as

follow: How much the local contrast of $\mathcal{D}(Y_{\text{PLEC}})$ is lowered compared to Y_S is measured.

$$\mathcal{M} = \left(\frac{\text{local contrast}(Y_S)}{\text{local contrast}(\mathcal{D}(Y_{\text{PLEC}})) + 10^{-7}}\right), \tag{3}$$

where the local contrast is the variance of a moving 5×5 window. Then, weight $\mathcal{W}$ can be obtained through a percentile thresholding of $\mathcal{M}$ per class. With $\mathcal{W}$ as a blending map, we blend I_{PLEC} and the contrast-enhanced image with CLAHE [6].

However, LCE from [19] has the following two limitations. First, LCE never considers the characteristics of our HVS. When people perceive an image, they focus on the salient object rather than the background. However, LCE determines the target area only. So, the contrast of the salient object might be lowered, and the background or noise might be amplified, which causes degradation in visibility. Fig. 4 shows this phenomenon. Second, since the old-fashioned CLAHE works independently of ambient light, there may be little effect from contrast enhancement at a certain illuminance.

In the next section, we provide a few solutions to overcome the limitations of [19], one by one. Fig. 5 illustrates the whole framework based on the solutions. We generate an ambient-light-adaptive pseudo-GT considering the correlation between luminance and chrominance. Using the pseudo-GT and CNN, image-content-aware contrast-enhancement of luminance and chrominance is achieved. Finally, by utilizing salient object detection, contrast in the salient object is further enhanced. Each step is trained independently in order. And only (c) and (d) steps are applied in inference.

B. VisibilityNet

To overcome the disadvantage from the correlation between chrominance and luminance not being considered in PGG from [19], we propose a new pseudo-GT generation network called VisibilityNet. VisibilityNet consists of the two steps as seen in Fig. 5 (a).

In Step 1, the luminance component (Y channel) is learned so that the contrast difference between $\mathcal{D}(Y_{\text{VN}})$ and Y_S is minimized. Like PGG's VENet, we adopt U-Net [39] as the backbone network. By increasing the number of channels corresponding to convolution, and by adding batch normalization, we achieved better stability in learning and minimized artifacts, which is demonstrated later in Section V. Loss function $\mathcal{L}_Y$ is as same as $\mathcal{L}_{\text{VENet}}$ [19] used in PGG, and the formula for $\mathcal{L}_Y$ is expressed by Eq. (4). Here, the first term learns the variance within a limited range to be as similar as possible to the original. In addition, the second term learns that the local region deteriorated due to $\mathcal{D}$ is additionally improved in terms of SSIM [40].

$$\mathcal{L}_Y = 2 - \frac{2\sigma_{Y_S\mathcal{D}(Y_{\text{VN}})} + \epsilon}{\sigma^2_{Y_S} + \sigma^2_{\mathcal{D}(Y_{\text{VN}})} + \epsilon} - \text{SSIM}(Y^m_S, \mathcal{D}(Y^m_{\text{VN}})) \tag{4}$$

In Step2, using U-Net and the degradation model of the structure from the previous step, the chrominance component (Cb/Cr channel) is learned so that contrast is enhanced considering ambient light while minimizing the chromaticity distance from the original. In addition, to learn the correlation with the Y channel from Step 1, the Y, Cb, and Cr channels of the source image and the Y channel from Step 1 are concatenated as input. Prior to designing an appropriate loss function, we need to understand the characteristics of CbCr channels. Fig. 6 visualizes the CbCr domain. Fig. 6 (a), representing CbCr in Cartesian coordinates, shows that learning through simple comparison of CbCr cannot consider both chromaticity and contrast. On the other hand, in Fig. 6 (b) showing CbCr in polar coordinate, each angle θ of Cb and Cr represents chromaticity and magnitude r represents contrast. So, we transform the CbCr channels to polar coordinates. As a result, color distortion is minimized, and chrominance contrast is enhanced according to the ambient light. The loss function for chrominance components, $\mathcal{L}_C$, consists of two terms. The first term is the angle loss to minimize the angle difference between $\mathcal{D}(C_{\text{VN}})$ and C_S. The angle loss is defined by using the cosine similarity loss [41] of each chrominance with L2 normalization applied, which is formulated in Eq. (5).

$$\mathcal{L}_{\text{angle}} = 1 - \frac{\mathcal{D}(C_{\text{VN}}) \cdot C_S}{||\mathcal{D}(C_{\text{VN}})|| \cdot ||C_S||} \tag{5}$$

The second term is the magnitude loss to minimize the contrast difference between $\mathcal{D}(C_{\text{VN}})$ and C_S. The magnitude loss is defined with Eq. (6) by applying SSIM loss [40] to chrominances:

$$\mathcal{L}_{\text{magnitude}} = \mathcal{L}_{\text{SSIM}}(\mathcal{D}(C_{\text{VN}}), C_S) \tag{6}$$

The total loss function of chrominance based on the two loss terms is defined by

$$\mathcal{L}_C = \lambda_1 \mathcal{L}_{\text{angle}} + \lambda_2 \mathcal{L}_{\text{magnitude}} \tag{7}$$

Here, λ_1 and λ_2 are hyperparameters that adjust color distortion reduction and contrast enhancement, respectively. We experimentally set λ_1 and λ_2 to 1.

Fig. 7 shows pseudo-GTs generated by this framework. I_P of PGG suffers from the wash-out phenomenon because chrominance is enhanced without regard for luminance. On the other hand, I_{VN} of VisibilityNet shows much better visual quality.

In summary, VisibilityNet effectively generates luminance and chrominance suitable for ambient light.

C. CONTENT-AWARE GLOBAL CONTRAST-ENHANCEMENT

In order to overcome the limitations of GCE of [19] caused by classification considering only average brightness, this section presents a content-aware GCE, illustrated in Fig. 5 (c).

First, we generate PLECs for each image, (that is, image-wise PLECs, I_{IW}), which is obtained by overfitting a pair of 'I_S-I_{VN}'. The independent learning process is illustrated in Fig. 5 (b). Note that PLECs are generated through a regression process for the S and V channels of the HSV color domain. To regress image-specific PLECs, enabling the

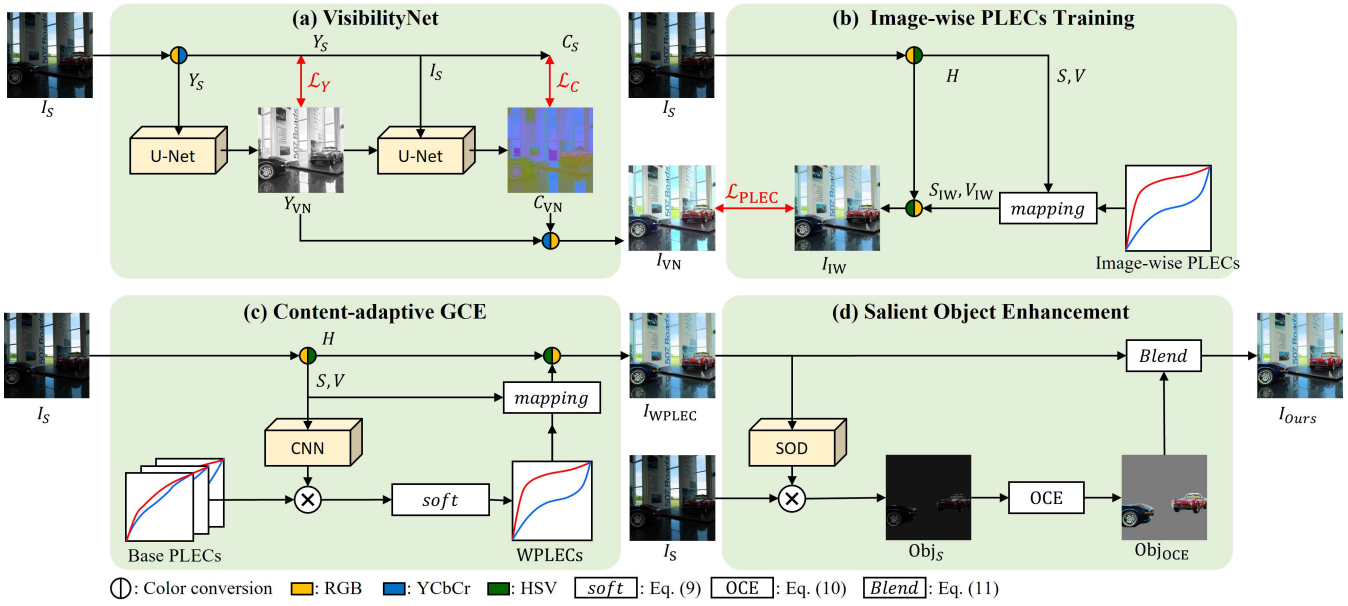

FIGURE 5. Overview of the proposed method. (a), (b), (c), and (d) are the framework of each step, respectively. Note that only (c) and (d) are applied in inference. Here, I_S means the source image. The luminance and chromiance of I_S are Y_S and C_S, respectively. HSV channels are represented by H, S, and V. (a) Y_{VN} and C_{VN} mean luminance and chrominance enhanced by VisibilityNet, respectively. I_{VN} is the generated pseudo-GT, and Y_{VN} and C_{VN} are combined. (b) S_{IW} and V_{IW} mean S and V channels enhanced with image-wise PLECs, respectively. H, S_{IW} and V_{IW} are combined to generate image I_{IW} enhanced with image-wise PLECs. (c) I_{WPLEC} is an image enhanced with WPLECs. (d) Obj_S is the salient object of the source image extracted by SOD. Obj_{OCE} means the object enhanced by OCE, and finally I_{Ours} means our final output.

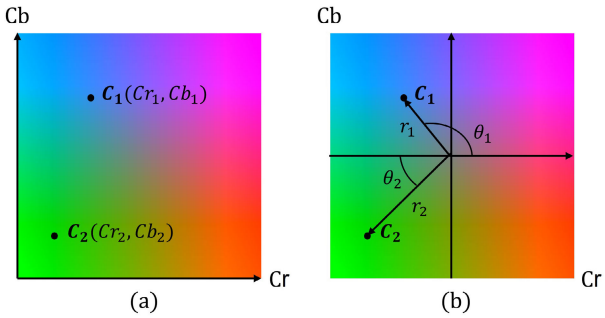

FIGURE 6. CbCr channels in coordinate systems. (a) Cartesian coordinate cannot consider both chromaticity and contrast of each chrominance (Cb or Cr). (b) With polar coordinates, we can check the chromaticity and contrast of each chrominance through θ and r.

FIGURE 7. (a) shows source images, (b) and (c) are outputs of PGG and VisibilityNet, respectively. Both (b) and (c) are enhanced according to 'sunlight' condition.

generation of I_{IW} similar to I_{VN}, it is necessary to calculate the color difference between the two images in the HSV color domain. Here, the HSV color format is converted to the Cartesian coordinate system to calculate the color difference ($x = sv \cdot \cos h$, $y = sv \cdot \sin h$, and $z = v$). Then, expanding based on the Euclidean distance, Eq. (2) is derived. Therefore, the loss function defined below quantifies the color difference between I_{IW} and I_{VN}.

$$\mathcal{L}_{PLEC} = \{(V_{VN} - V_{IW})^2 + S_{VN}^2 V_{VN}^2 + S_{IW}^2 V_{IW}^2 - 2S_{VN}S_{IW}V_{VN}V_{IW}\cos(H_{VN} - H)\}^{1/2}, \quad (8)$$

where H_{VN}, S_{VN}, and V_{VN} indicate the H, S, and V channels of I_{VN}, respectively. H is the H channel of I_S, and S_{IW} and V_{IW} are the S and V channels of I_{IW}. The slope vector of image-wise PLECs is defined by Eq. (9).

$$P_j = \sigma(A_j) \times 8, \quad j \in \{S, V\} \quad (9)$$

We set the total sum of P_j to 8 by adding softmax (σ) to Eq. (2) and multiplying it by 8, which is the length of A_j. This way, we can constrain pixel values to be between 0 and 255. Softmax prevents a specific slope of P_j from rapidly changing or from approaching zero, and it enables learning that considers the correlation between control points. This is verified in Section V-B. Fig. 8 (a) illustrates image-wise PLECs. Note that average brightness and image-wise PLECs

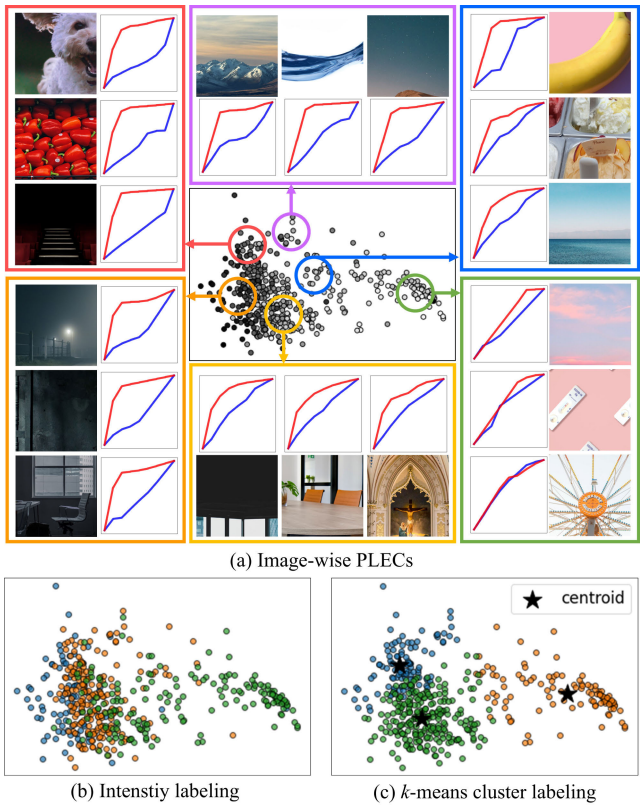

(a) Image-wise PLECs

(b) Intenstiy labeling

(c) k-means cluster labeling

FIGURE 8. **(a) Visualizations of image-wise PLECs in which they are projected onto a two-dimensional space using PCA. Each point is a projected image-wise PLECs, and the color of each point indicates the average intensity of the input image. (b) Classification of image-wise PLECs when labeling them in terms of average brightness. (c) Classification of image-wise PLECs through k-means clustering.**

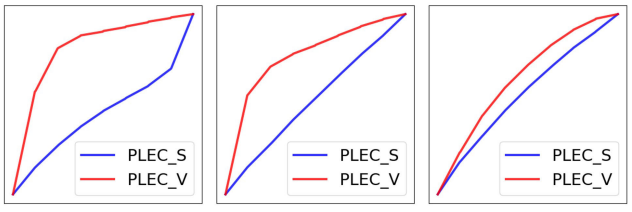

Base PLEC-1 Base PLEC-2 Base PLEC-3

FIGURE 9. **Example of the base PLECs.**

have a low correlation, and the decision boundary of the intensity-based classifier is unclear, as seen in Fig. 8(b). This demonstrates that PLEC regression through average brightness-based classification has its limitations.

To solve this problem, we propose a novel regression framework, i.e., weighted PLECs (WPLECs) to improve images in a content-adaptive fashion. We construct the base PLECs and regress WPLECs in the form of a weighted sum of the base PLECs, as illustrated in Fig. 5 (c). To determine the base PLECs, we apply k-means clustering to the image-wise PLECs. Here, we set k to 3 for a fair comparison with our prior work. Fig. 8 (c) shows that the decision boundary is still unclear, but the centroids (black stars) quantize the overall distribution well. Therefore, we use the centroid of each cluster as the base PLECs (Fig. 9). Then, to estimate the weights of base PLECs by taking image content into account, we use a modified VGG-11 [42]. Some modifications of the VGG-11 model are as follows: The first is to use two-dimensional input. Since PLECs are regressed on S and V channels, the CNN model receives the S and V channels as input. The second modification is to change the activation function from a ReLU to tanh. In order to generate weights of more flexible base PLECs, we use tanh with a range of [-1, 1] instead of ReLU that always clips negatives to 0. After matrix multiplication between the weights calculated by VGG-11 and the base PLECs, a softmax operation is applied to obtain the WPLECs for S and V channels. The loss function for the WPLECs adopts the L1 loss between the image-wise PLECs and the WPLECs derived from the weight×base PLECs.

Therefore, unlike PLECs of [19], WPLECs enables to enhance global contrast considering image content.

D. SALIENT OBJECT ENHANCEMENT

In order to solve the limitation of the previous LCE step (in which HVS is irrelevant), we propose salient object enhancement for improving the visibility of the main object(s) in an image. SOE consists of salient object detection (SOD) and object contrast-enhancement (OCE). The overall framework of SOE is illustrated in Fig. 5 (d).

To detect the main object, we utilize the SOD technique using deep learning. As a computer vision task that extracts the most attractive region in an image [43], SOD aims to simulate HVS, which usually focuses on the main object(s). Comparing the performance of several SOD techniques, we chose a scene-context-aware SOD model [20]. In general, SOD models do not work on images with low brightness or low contrast. So, we input I_{WPLEC} (with WPLEC applied) to the SOD model. Then, mask $\mathcal{M}$ of the salient object, i.e., the prediction map is obtained through the SOD model.

Next, we propose OCE to enhance visibility of the salient object(s) according to ambient light. In order to avoid over-enhancement of the salient object(s), we define Obj_S by multiplying I_S (instead of I_{WPLEC}) by $\mathcal{M}$, and then use Obj_S as input for OCE. Then, OCE is performed with WPLECs that is multiplied by a pre-determined coefficient. OCE is defined by Eq. (10). Here, *coef* is multiplied to further improve the visibility of the salient object against the background. In other words, considering the human visual system that focuses more on the salient object, the effect of improving visibility is maximized.

$$\mathrm{OCE} = \begin{cases} \mathrm{WPLECs} \times \mathit{coef}, & (\mathit{coef} \geq 1) \\ \mathrm{WPLECs}, & (\mathrm{otherwise}) \end{cases} \tag{10}$$

where *coef* is set to $\log(\mathrm{WPLECs}/\sigma + 1) + \alpha$, σ is set to 2, and α is set to 2.5. An ablation study of OCE is discussed in Section V-C.

Finally, I_{Ours} is obtained by blending the salient object $\mathrm{Obj}_{\mathrm{OCE}}$ with OCE applied and the background from I_{WPLEC}.

The blending procedure is defined by Eq. (11).

$$Blend = \mathcal{M}_b \mathrm{Obj}_{\mathrm{OCE}} + (1 - \mathcal{M}_b) I_{\mathrm{WPLEC}} \quad (11)$$

where $\mathcal{M}_b$ denotes the blending map generated by applying a well-known Gaussian filter to $\mathcal{M}$. When blending an enhanced salient object and background, artifacts may occur at object boundaries when discrete binary masks are used. To prevent this, we use a Gaussian mask to naturally synthesize the boundary between the salient object and the background.

Therefore, the proposed method, which is composed of GCE that considers ambient light as well as image content, and LCE to further enhance the salient object(s), accomplishes visibility improvement suitable for our HVS.

IV. EXPERIMENTS

This section concentrates on qualitative comparison with previous methods. Section IV-A describes the experiment configuration, and Section IV-B shows the results in terms of mean opinion score.

A. EXPERIMENTAL CONFIGURATION

1) DATASET

The dataset for PGG and GCE learning is from our prior work, consisting of 600 real-world scenes with various brightness ranges. The training set was built through web crawling and consists of 500 images in total. The test set comprised 100 images, 60 sampled from Ward's HDR dataset [44], which is also consisted of real-world images, and 40 obtained by web crawling. Here, the image-wise PLECs has a dimension size of 16 including slopes for S and V.

2) AMBIENT LIGHT

We considered three ambient light conditions for this experiment: The strongest illuminance 'sunlight', the medium illuminance 'overcast', and the weakest illuminance 'office', corresponding to 10,000 lux, 2,000 lux, and 500 lux, respectively. For qualitative evaluation, the degraded images due to external illuminance are visualized through a degradation model. Also, the experimental environment for MOS evaluation was set to 'sunlight' condition, which is the strongest illuminance among ambient light condition. For this experiment, we used a light box that can adjust illuminance up to 10 levels.

3) MOS

MOS was measured on nine image sets. Each set was composed by randomly choosing output from the proposed and other methods. The visibility of each image scored between 1 (poor) and 5 (very good), and the average score of all image sets became the final score. Unfortunately, since the degradation model highly depends on the display, experiments with various commercial displays would cost too much. So, we adopted the Samsung Galaxy Tab S7 as the target display for this paper. Official parameters that can be found out from the manufacturer are set as display parameters (i.e., maximum contrast, brightness, etc.) for degradation modeling.

TABLE 1. MOS evaluation for the 'sunlight' condition.

Image	Source	DATMO	Prior	Ours
MOS	1.54	3.24	3.52	4.10

The total number of volunteer participants for MOS evaluation was 11 (nine males and two females) aged 24 to 30.

B. QUALITATIVE EVALUATION

For benchmarking, we adopted several previous works: SEF [8], which is a general contrast-enhancement technique; SCI [27] and SNR [28], which are low-light image enhancement techniques; DATMO [32], which has the only code available among the ambient-light adaptive image enhancement techniques; and our prior work [19]. Here, we only utilize the official code for fairness of comparison. Here, the result image for each method is expressed by putting the corresponding method name in the subscript of I.

Fig. 10 shows the qualitative evaluation results. First, an LLIE technique I_{SCI} significantly lost image information due to over-enhancement in 'office' and 'sunlight'. In 'overcast', I_{SCI} was washed-out compared to the original image. In case of I_{SNR}, the parking lot was inappropriately improved in 'office'. I_{SNR} was over-enhanced in 'overcast'. In 'sunlight', the color of the car and sky area was not maintained. I_S suffered from some artifacts and distortions in the sky area under the 'office' and 'sunlight' conditions. I_{SEF} suffered from some artifacts and distortions in the sky area under the 'office' and 'sunlight' conditions. Also, in the 'overcast' condition, halo artifacts occurred around the candles. With I_{DATMO}, global luminance was enhanced under 'office' and 'sunlight' conditions, but the sky area washed-out. In the 'overcast' condition, I_{DATMO} showed halo artifacts around the candles, like I_{SEF}. With I_{Prior} to which [19] was applied, the wash-out phenomenon under 'office' and 'sunlight' conditions was mitigated, and chrominance was better enhanced, compared to I_{DATMO}. Also, the halo artifacts under 'overcast' condition were properly resolved. However, I_{Prior} still has limitations. In (a) of office, the contrast of a salient object, e.g., car, is not sufficiently improved, so the boundary between the car and the shadow is not well distinguished in (b). In (b) of overcast, we can observe a wash-out phenomenon in which color information is not improved as much as brightness information when compared to I_S of (a). In (a) of 'sunlight', the red and blue cars are not sufficiently improved, so the information of each car is lost in (b). Especially in the blue car, we cannot distinguish between the object and the floor. However, in I_{Ours}, the above problems are successfully solved. From the qualitative results of I_{Ours}, we can find that WPLECs

FIGURE 10. Qualitative comparison of the proposed method with previous works. In each condition, (a) is the enhanced image by each technique, and (b) results from simulating the image degraded by each condition using degradation model, $\mathcal{D}$.

and SOE of the proposed method effectively improved the luminance and chrominance. Qualitative evaluations from experiments indicate that traditional image enhancement techniques that neglect ambient light yield unsatisfactory results. In contrast, the proposed method demonstrates adaptive image quality improvement, effectively accommodating the image's specific characteristics across diverse ambient lighting conditions.

Next, to prove that the proposed method works well even in a real environment, Table 1 shows evaluation results in terms of MOS. In this experiment, the visibility scores are averaged at the actual 'sunlight' illuminance where visibility improvement is most difficult.

As benchmarking techniques, we set up DATMO and our prior work because they pursue the same task as ours, that is, image enhancement technique considering external illumination. Source images show the lowest score due to degradation by ambient light. DATMO considers ambient light, so DATMO usually scores 1.7 higher than source images. However, since DATMO considers only luminance and not chrominance, it faces a so-called wash-out phenomenon. Thus, DATMO scores about 0.3 lower than even our prior work. On the other hand, the proposed method pursues salient object enhancement considering perception as well as luminance/chrominance improvement considering image content. Therefore, the proposed method achieves

TABLE 2. Quantitative results of each NR metrics. Note: SUN=sunlight, OVC=overcast, OFC=office.

Metric	NIQE↓ (dB)			MUSIQ↑		
Condition	OFC	OVC	SUN	OFC	OVC	SUN
$\mathcal{D}(I_S)$	4.690	4.738	4.796	34.357	34.323	33.437
$\mathcal{D}(I_{\text{SEF}})$	4.604	4.646	4.762	34.454	34.420	34.405
$\mathcal{D}(I_{\text{SCI}})$	5.411	4.692	4.384	31.926	31.948	32.119
$\mathcal{D}(I_{\text{SNR}})$	8.613	7.956	7.354	26.808	26.879	27.017
$\mathcal{D}(I_{\text{DATMO}})$	3.991	4.103	4.347	37.090	36.136	34.799
$\mathcal{D}(I_{Prior})$	3.934	4.017	4.178	37.737	36.720	35.927
$\mathcal{D}(I_{Ours})$	3.953	3.960	4.079	38.021	37.630	36.587

the best MOS score while further improving the visibility of salient object(s). To summarize, compared to source, DATMO, and our prior work, the proposed method provided higher MOS by 2.56, 0.86, and 0.58 for the three illuminance conditions, respectively.

C. QUANTITATIVE EVALUATION

There is no reference image for our result I_{Ours}. So, to quantitatively evaluate I_{Ours}, we employ two no-reference (NR) metrics, i.e., NIQE [45] and MUSIQ [46]. NIQE measures the quality of an image by computing the degree of distortion (blur, artifact, etc.) of the image. The lower the NIQE score, the better the quality. MUSIQ transforms an input image into multi-scale representations with global and local views to capture image quality at different granularities. The higher the MUSIQ score, the better the quality. Since we aim to improve the visibility of images that are degraded by ambient light, we measured metric scores after applying a degradation model $\mathcal{D}$ to the resulting images. Table 2 shows the results. As in the qualitative evaluation, all techniques have lower scores as the ambient light intensity increases. That is, visibility is reduced. First, the NIQEs of $\mathcal{D}(I_{\text{SCI}})$ and $\mathcal{D}(I_{\text{SNR}})$ improved by SCI and SNR, which are LLIE techniques, are 4.829 and 7.974 on average, respectively, and their MUSIQs are 31.998 and 26.901 on average, respectively. That is, of $\mathcal{D}(I_{\text{SCI}})$ and $\mathcal{D}(I_{\text{SNR}})$ are worse than $\mathcal{D}(I_S)$ to which no improvement is applied, by 1.86% and 68.19%, respectively in terms of NIQE and by 6.00% and 20.97%, respectively in terms of MUSIQ. The LLIE techniques show such results because they target only low-light images regardless of ambient light, i.e., because their purpose is clearly different from ours. Next, in the case of $\mathcal{D}(I_{\text{SEF}})$ improved by SEF, which is a general contrast-enhancement technique that does not consider ambient light, NIQE and MUSIQ were 1.47% and 1.14% better than $\mathcal{D}(I_S)$, respectively. However, this is insignificant. $\mathcal{D}(I_{\text{DATMO}})$, which enhances only luminance by considering ambient light, showed better NIQE and MUSIQ by 13.10% and 5.78%, respectively, than $\mathcal{D}(I_S)$. In the case of $\mathcal{D}(I_{Prior})$ considering chrominance as well as luminance, NIQE increased by 14.72% and MUSIQ by 7.49% compared to $\mathcal{D}(I_S)$. Thus, I_{Prior} provides better visibility compared to DATMO. Finally, in the case of I_{Ours}, NIQE improved by 15.69% and MUSIQ by 9.91% compared to $\mathcal{D}(I_S)$. This is the most significant visibility improvement. Therefore, it is experimentally proven that the proposed method has the best image quality in any ambient light environment.

TABLE 3. Comparisons of model complexities.

Method	run-time (ms)	num of params (M)	model size (KB)	device
SEF	268	-	-	CPU
DATMO	167	-	-	CPU
SCI	1.7	0.0003	43	GPU
SNR	51.6	39	152,855	GPU
Prior	97	-	-	CPU
Ours	63.8	70	270,340	GPU

To analyze the complexity of each model, we compare the run-time per 1M pixel, the number of model parameters, and the model size. Table 3 shows the analysis result. SEF, DATMO, and prior work operate rule-based, so they have no learnable parameters. Therefore, we measured run-times on a CPU (i.e. Intel CPU i7-8700@3.2GHz). Note that here, PLECs of prior work are regressed through deep learning, but are implemented in the form of a so-called 'Look Up Table' by saving slopes during inference. On the other hand, SCI, SNR, and Ours based on deep learning were tested on a GPU (i.e., NVIDIA Gefore 1080 Ti).

V. ABLATION STUDY

A. VisibilityNet

This section compares the performance of PGG [19] and VisibilityNet. First, Fig. 11 demonstrates the structural effect from VisibiltyNet. That is, it compares Y_P and Y_{VN}, which are the luminance components output from VENet and VisibilityNet, respectively. VENet did not fully consider image content due to an insufficient number of channels and the absence of batch normalization. This makes learning by VENet unstable, and artifacts were eventually observed in the sky area (top row) and shadows area (bottom row) of Y_P. On the other hand, in VisibilityNet, the artifact problem was mitigated by sufficiently considering image content along with stable learning.

Next, we compare the chrominance components produced by PGG's *CF* and by VisibilityNet. Here, to see only chrominance, luminance was set to Y_{VN}. Fig. 12 shows the chrominance output from both methods. I_{VN} did not suffer from the wash-out phenomenon, compared to I_P.

Therefore, VisibilityNet generates a pseudo-GT adaptive to the ambient light and image content, providing content-aware GCE.

B. CONTENT-AWARE GLOBAL CONTRAST-ENHANCEMENT

In this experiment, we used I_{IW} as the reference image and employed PSNR and SSIM as evaluation metrics. First, take a look at Fig. 13, which shows the effect from softmax. Softmax makes curves smoother by preventing slopes from becoming zero or changing rapidly in a specific section, as seen in Fig. 13 (a). Softmax mitigates the contour artifacts and saturation as in the red boxes of I_{IW} in Fig. 13 (b).

Second, in order to examine the effect from considering image content, Fig. 14 analyzes I_{IPLEC} and I_{WPLEC}

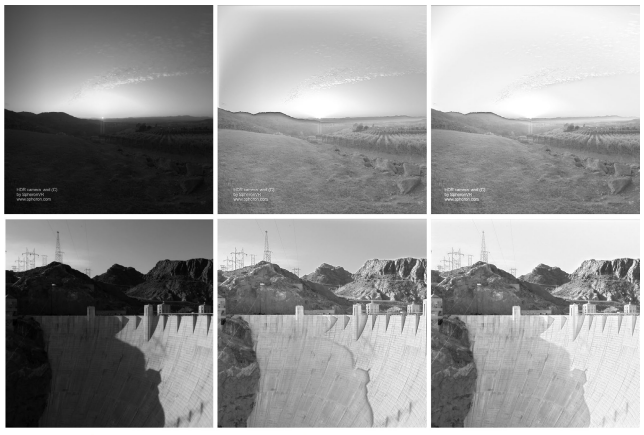

FIGURE 11. Performance comparison of PGG's VENet and VisibilityNet under 'sunlight' condition. (a), (b) and (c) show the Y component of the source image, the result from VENet of our prior work, and the result from VisibilityNet, respectively. Both (b) and (c) are enhanced according to 'sunlight' condition.

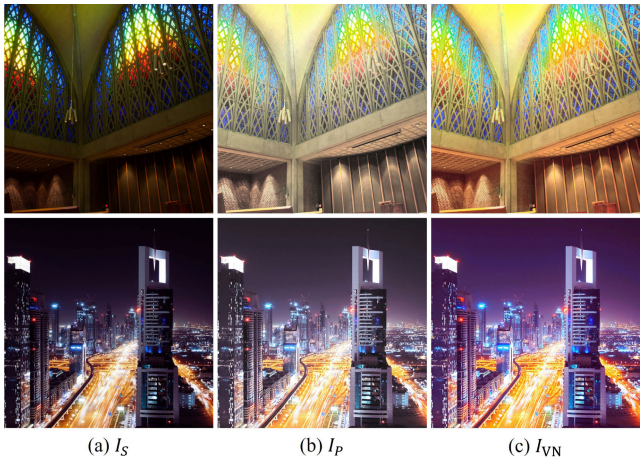

FIGURE 12. (a) is the source image. (b) and (c) shows the output of PGG and VisibilityNet, respectively. The top and bottom rows correspond to 'sunlight' and 'overcast' environments, respectively.

from IPLECs and WPLECs, respectively. Here, IPLECs is regressed through GCE from [19] using I_{VN}. I_{IPLEC} provided better contrast than I_S. However, it shows under-enhancement under 'office' and 'overcast' condition, and suffers from over-enhancement under 'sunlight' (red boxes). On the other hand, I_{WPLEC} stably enhanced both luminance and chrominance without under- and over-enhancement. In addition, Table 4 proves that I_{WPLEC} had a higher MOS than I_{IPLEC}, indicating that I_{WPLEC} provides better visibility even in an real environment. Third, Table 5 shows that the PSNR and SSIM of I_{WPLEC} increased by 1.87dB and 0.005 on average, respectively, compared to I_{IPLEC}. This proves that image content is a better criterion for classification than average brightness. As a result, we conclude that content-aware WPLECs quantitatively and qualitatively outperforms IPLECs.

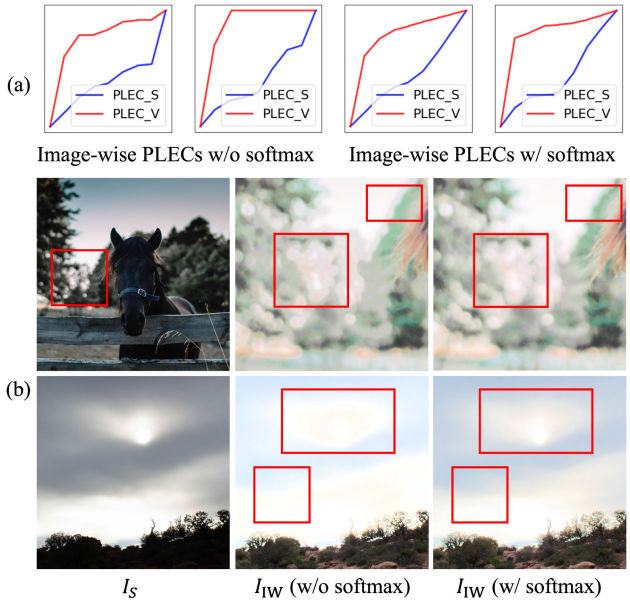

FIGURE 13. The effect of softmax. (a) curves with or without softmax, and (b) results from the curves in (a).

TABLE 4. MOS comparison of IPLECs and WPLECs under 'sunlight' condition.

Image	Source	IPLECs	WPLECs
MOS	2.08	3.27	3.49

TABLE 5. Comparison of PSNR and SSIM from IPLECs and WPLECs according to ambient light. Note: SUN=sunlight, OVC=overcast, OFC=office.

Metric	PSNR↑ (dB)			SSIM↑		
Condition	OFC	OVC	SUN	OFC	OVC	SUN
I_{IPLEC}	33.37	30.65	27.79	0.99	0.98	0.97
I_{WPLEC}	36.29	31.79	29.32	0.99	0.98	0.98

TABLE 6. MOS of SOE under 'sunlight' condition.

Image	Source	WPLECs	WPLECs+LCE	WPLECs+SOE
MOS	1.58	3.12	2.91	4.04

In addition, Fig. 15 analyzes quantitative performance according to k from content-aware GCE. In this experiment, the ambient light was 'sunlight'. We can see that PSNR and SSIM tended to increase as k increased. Here, k=7 was the best, but the performance gap based on k was not so significant. Therefore, we set k to 3 considering the training cost.

C. SALIENT OBJECT ENHANCEMENT

This section presents two experimental results from SOE. The first experiment was to verify the effect of OCE. Specifically, an ablation study according to the OCE coefficient is conducted. Here, we considered three types of coefficient. The first was 1 as the most trivial. This means that OCE applied WPLECs reflecting the object characteristics as is.

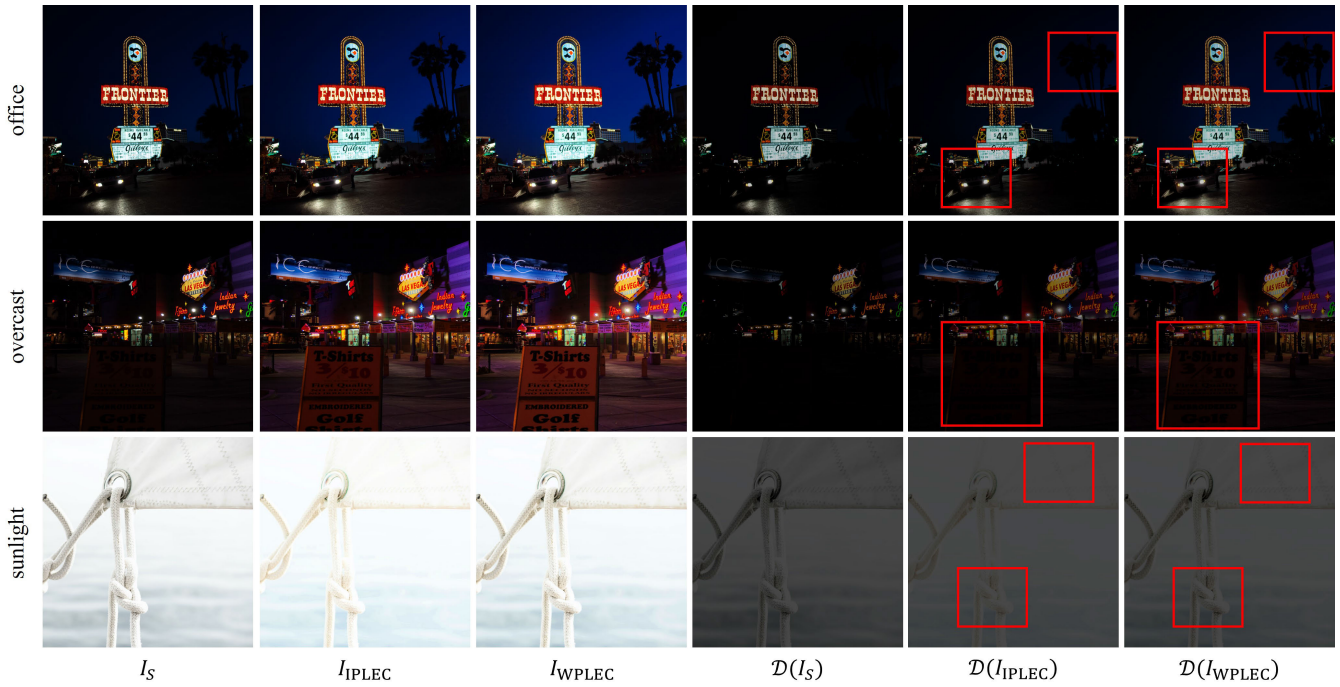

FIGURE 14. Comparison of IPLECs and WPLECs. The top, middle, bottom rows correspond to the 'office', 'overcast', and 'sunlight' environments, respectively.

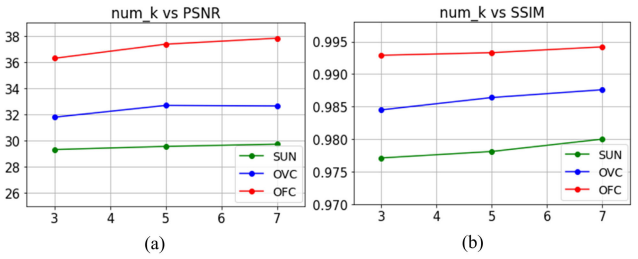

FIGURE 15. Performance according to k under 'sunlight' condition (k=3, 5, 7) (a) and (b) show PSNR and SSIM, respectively, when WPLECs is trained according to k.

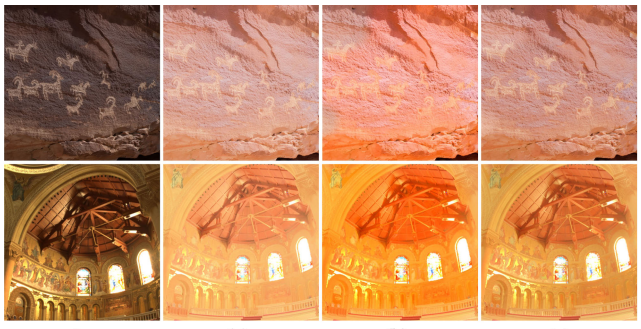

FIGURE 16. Images with OCE applied in a 'sunlight' condition. (a), (b), and (c) correspond to three coefficients, i.e., 1, 1.2, and the logarithmic function, respectively.

The second coefficient experimentally explored was 1.2. The third coefficient, *coef*, was adaptively determined with a logarithmic function. This maintains WPLECs from a point where *coef* becomes smaller than WPLECs, which prevents the under-enhancement phenomenon.

Fig. 16 compares OCE results where the above three coefficients were applied. For clearer observation, we show only salient objects cropped from the resulting images. Fig 16 (a) has better global luminance and chrominance than I_S, but deteriorated in terms of object contrast and detail. Fig 16 (b) had more brightness and sharper saturation than Fig. 16 (a), but tended towards over-enhancement. On the other hand, Fig. 16 (c), to which the proposed OCE was applied, preserved the original mural pattern (top row) and maintained details of the structure well (bottom row). At the same time, contrast improved, resulting in much better visibility.

The second experiment compared SOE with LCE of [19]. The two methods were applied to I_{WPLEC}. Fig. 17 shows the results, as well as an additional image to which $\mathcal{D}$ was applied. Note that salient objects are highlighted properly.

Under 'office' condition, $I_{\text{WPLEC+LCE}}$ became darker than I_{WPLEC} because of the characteristics of CLAHE. So, when $\mathcal{D}$ was applied, visibility was somewhat decreased. On the other hand, looking at the petals of $I_{\text{WPLEC+SOE}}$, we observe better contrast than I_{WPLEC}. Under 'overcast' condition, the face area of $I_{\text{WPLEC+LCE}}$ hardly changed, compared to I_{WPLEC}. Instead, the contrast of the background seems to have improved. Even in $\mathcal{D}(I_{\text{WPLEC+LCE}})$, it is difficult to recognize faces as in $\mathcal{D}(I_{\text{WPLEC}})$. But $I_{\text{WPLEC+SOE}}$ properly enhanced the face area as a salient object. Also, the face area in

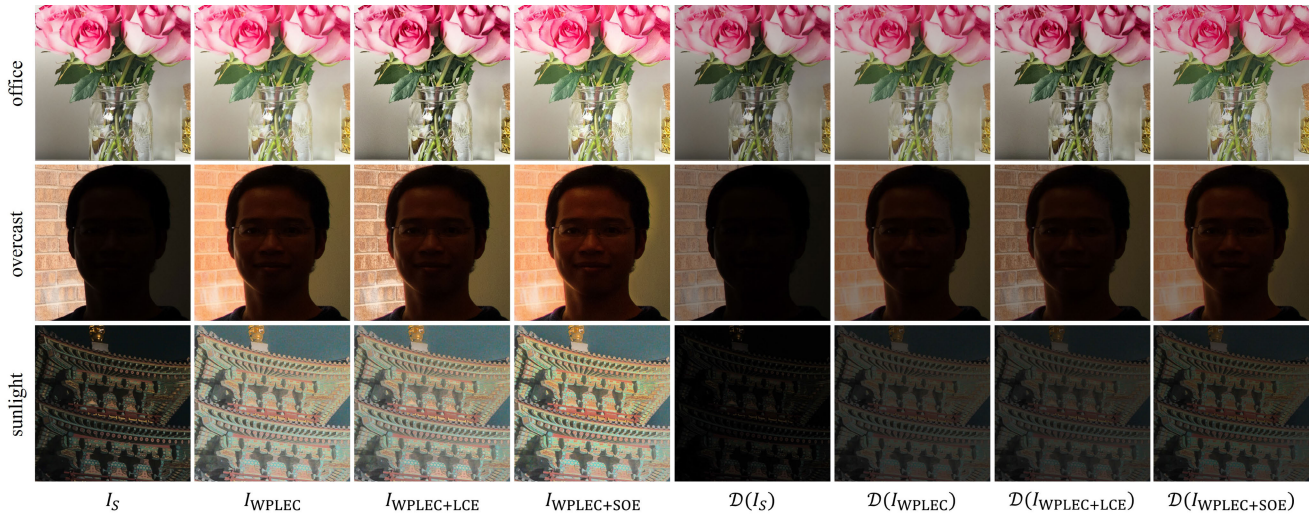

FIGURE 17. Visual quality comparison of LCE and SOE.

$\mathcal{D}(I_{\text{WPLEC+SOE}})$ is recognizable. Under 'sunlight' condition, the salient object (the building) from I_{WPLEC} does not show acceptable contrast. Although $I_{\text{WPLEC+LCE}}$ was better overall than I_{WPLEC}, $\mathcal{D}(I_{\text{WPLEC+LCE}})$ produced less visibility than $\mathcal{D}(I_{\text{WPLEC}})$. On the other hand, the contrast of the building in $I_{\text{WPLEC+SOE}}$ was greatly enhanced, and the building area is clearly recognized in $\mathcal{D}(I_{\text{WPLEC+SOE}})$.

Additionally, Table 6 evaluated the proposed SOE in terms of MOS. Note that SOE provided a MOS 1.13 higher than LCE. This proves that SOE outperforms LCE even in the wild.

VI. DISCUSSION

This paper presents a software solution to mitigate the phenomenon that the displayed image is perceived as darker than the source image due to our human visual system when viewing the displayed image in an ambient light environment. However, various distortions (e.g., noise) other than ambient lighting issue can occur. Unfortunately, until now, we have not been able to find a model that simulates those distortions. If such a degradation model is available in the future, a method for improving image quality adaptive to various distortions can be devised.

Next, the degradation model we used here considers the brightness (lux) of ambient light and the display specification to simulate how the displayed image can be perceived at a specific lux. Accordingly, we designed a model with only the lux of the ambient light as a parameter, and used a lighting box for experiments according to lux. That is, only artificial light sources are considered in this paper. As a result, the proposed method has limitations in handling various cases (e.g., non-uniform lighting, backlit scenarios, etc) that can occur in natural light sources. Since the variability between natural light source and artificial light source definitely exists, research on this will be needed in the future.

VII. CONCLUSION

Our proposed framework presents an adaptive contrast-enhancement approach that enhances visibility in diverse ambient light conditions while considering image content. Initially, a pseudo-ground-truth (GT) dataset is generated, optimized for external illuminance, through degradation modeling and neural networks. Subsequently, utilizing the generated dataset and a convolutional neural network (CNN) model, mapping curves are trained, considering the image content. Consequently, global luminance and chrominance are improved using these mapping curves. Moreover, leveraging salient object detection techniques that simulate the human visual system (HVS), the contrast of salient object(s) is further enhanced. By conducting qualitative evaluations of image quality, we establish the superiority of the proposed method over conventional approaches (including our previous work) across diverse ambient light environments. Furthermore, MOS evaluations demonstrate that the proposed method significantly enhances visibility compared to conventional methods, even in real-world scenarios. In conclusion, this paper presents an adaptive solution for visibility improvement that effectively considers both ambient light conditions and image content.

However, the proposed method does have certain limitations. Firstly, it only considers three specific ambient light conditions, potentially limiting its generalizability. Secondly, the modified VGG-11 model used in content-adaptive global contrast enhancement (GCE) is not specifically optimized for ambient light and may be too computationally heavy for mobile environments. Thirdly, there is scope for enhancing the performance of object contrast enhancement (OCE) specifically for salient objects. Overcoming these limitations will be the focus of our future work.

ACKNOWLEDGMENT

(Junmin Lee and Heejin Lee contributed equally to this work.)

REFERENCES

[1] H. Zeng, J. Cai, L. Li, Z. Cao, and L. Zhang, "Learning image-adaptive 3D lookup tables for high performance photo enhancement in real-time," *IEEE Trans. Pattern Anal. Mach. Intell.*, vol. 44, no. 4, pp. 2058–2073, Apr. 2022.

[2] G.-D. Fan, B. Fan, M. Gan, G.-Y. Chen, and C. L. P. Chen, "Multiscale low-light image enhancement network with illumination constraint," *IEEE Trans. Circuits Syst. Video Technol.*, vol. 32, no. 11, pp. 7403–7417, Nov. 2022.

[3] C. Liu, F. Wu, and X. Wang, "EFINet: Restoration for low-light images via enhancement-fusion iterative network," *IEEE Trans. Circuits Syst. Video Technol.*, vol. 32, no. 12, pp. 8486–8499, Dec. 2022.

[4] S. H. Kim, "Device and method for controlling LCD backlight," U.S. Patent 6 812 649, Nov. 2, 2004.

[5] J.-M. Kim, C.-H. Son, C.-H. Lee, and Y.-H. Ha, "Illuminant adaptive color reproduction based on lightness adaptation and flare for mobile phone," in *Proc. Int. Conf. Image Process.*, Oct. 2006, pp. 1513–1516.

[6] A. M. Reza, "Realization of the contrast limited adaptive histogram equalization (CLAHE) for real-time image enhancement," *J. VLSI Signal Process.-Syst. Signal, Image, Video Technol.*, vol. 38, no. 1, pp. 35–44, Aug. 2004.

[7] Y.-F. Liu, J.-M. Guo, and J.-C. Yu, "Contrast enhancement using stratified parametric-oriented histogram equalization," *IEEE Trans. Circuits Syst. Video Technol.*, vol. 27, no. 6, pp. 1171–1181, Jun. 2017.

[8] C. Hessel and J.-M. Morel, "An extended exposure fusion and its application to single image contrast enhancement," in *Proc. IEEE Winter Conf. Appl. Comput. Vis. (WACV)*, Mar. 2020, pp. 137–146.

[9] N. Hayat and M. Imran, "Detailed and enhanced multi-exposure image fusion using recursive filter," *Multimedia Tools Appl.*, vol. 79, nos. 33–34, pp. 25067–25088, Sep. 2020.

[10] J. Li, J. Liu, S. Zhou, Q. Zhang, and N. K. Kasabov, "Learning a coordinated network for detail-refinement multiexposure image fusion," *IEEE Trans. Circuits Syst. Video Technol.*, vol. 33, no. 2, pp. 713–727, Feb. 2023.

[11] Z. Rahman, P. Yi-Fei, M. Aamir, S. Wali, and Y. Guan, "Efficient image enhancement model for correcting uneven illumination images," *IEEE Access*, vol. 8, pp. 109038–109053, 2020.

[12] Z. Rahman, Z. Ali, I. Khan, M. I. Uddin, Y. Guan, and Z. Hu, "Diverse image enhancer for complex underexposed image," *J. Electron. Imag.*, vol. 31, no. 4, May 2022, Art. no. 041213.

[13] Z. Rahman, M. Aamir, Z. Ali, A. K. J. Saudagar, A. AlTameem, and K. Muhammad, "Efficient contrast adjustment and fusion method for underexposed images in industrial cyber-physical systems," *IEEE Syst. J.*, early access, Apr. 24, 2023, doi: 10.1109/JSYST.2023.3262593.

[14] L. Zhu, W. Yang, B. Chen, F. Lu, and S. Wang, "Enlightening low-light images with dynamic guidance for context enrichment," *IEEE Trans. Circuits Syst. Video Technol.*, vol. 32, no. 8, pp. 5068–5079, Aug. 2022.

[15] Q. Ma, Y. Wang, and T. Zeng, "Retinex-based variational framework for low-light image enhancement and denoising," *IEEE Trans. Multimedia*, early access, Jul. 29, 2022, doi: 10.1109/TMM.2022.3194993.

[16] Z. Rahman, Y.-F. Pu, M. Aamir, and S. Wali, "Structure revealing of low-light images using wavelet transform based on fractional-order denoising and multiscale decomposition," *Vis. Comput.*, vol. 37, no. 5, pp. 865–880, May 2021.

[17] C. Guo, C. Li, J. Guo, C. C. Loy, J. Hou, S. Kwong, and R. Cong, "Zero-reference deep curve estimation for low-light image enhancement," in *Proc. IEEE/CVF Conf. Comput. Vis. Pattern Recognit. (CVPR)*, Jun. 2020, pp. 1777–1786.

[18] H. Su, C. Jung, S. Wang, and Y. Du, "Readability enhancement of displayed images under ambient light," *IEEE Trans. Circuits Syst. Video Technol.*, vol. 28, no. 7, pp. 1481–1496, Jul. 2018.

[19] H. Lee, J. Lee, S. Jeong, S. Lee, S. Yu, J. Heo, and B. C. Song, "Image enhancement for improved visibility of digital displays under the sunlight," in *Proc. IEEE Int. Conf. Image Process. (ICIP)*, Oct. 2022, pp. 3918–3922.

[20] A. Siris, J. Jiao, G. K. L. Tam, X. Xie, and R. W. H. Lau, "Scene context-aware salient object detection," in *Proc. IEEE/CVF Int. Conf. Comput. Vis. (ICCV)*, Oct. 2021, pp. 4136–4146.

[21] S.-C. Huang, F.-C. Cheng, and Y.-S. Chiu, "Efficient contrast enhancement using adaptive gamma correction with weighting distribution," *IEEE Trans. Image Process.*, vol. 22, no. 3, pp. 1032–1041, Mar. 2013.

[22] H. Li, T. N. Chan, X. Qi, and W. Xie, "Detail-preserving multi-exposure fusion with edge-preserving structural patch decomposition," *IEEE Trans. Circuits Syst. Video Technol.*, vol. 31, no. 11, pp. 4293–4304, Nov. 2021.

[23] W. Ye, T. Yan, J. Gao, and Y. Yang, "LFIENet: Light field image enhancement network by fusing exposures of LF-DSLR image pairs," *IEEE Trans. Comput. Imag.*, vol. 9, pp. 620–635, 2023.

[24] J. Li, X. Feng, and Z. Hua, "Low-light image enhancement via progressive-recursive network," *IEEE Trans. Circuits Syst. Video Technol.*, vol. 31, no. 11, pp. 4227–4240, Nov. 2021.

[25] Y. Ren, Z. Ying, T. H. Li, and G. Li, "LECARM: Low-light image enhancement using the camera response model," *IEEE Trans. Circuits Syst. Video Technol.*, vol. 29, no. 4, pp. 968–981, Apr. 2019.

[26] K. Xu, H. Chen, C. Xu, Y. Jin, and C. Zhu, "Structure-texture aware network for low-light image enhancement," *IEEE Trans. Circuits Syst. Video Technol.*, vol. 32, no. 8, pp. 4983–4996, Aug. 2022.

[27] L. Ma, T. Ma, R. Liu, X. Fan, and Z. Luo, "Toward fast, flexible, and robust low-light image enhancement," in *Proc. IEEE/CVF Conf. Comput. Vis. Pattern Recognit. (CVPR)*, Jun. 2022, pp. 5627–5636.

[28] X. Xu, R. Wang, C.-W. Fu, and J. Jia, "SNR-aware low-light image enhancement," in *Proc. IEEE/CVF Conf. Comput. Vis. Pattern Recognit. (CVPR)*, Jun. 2022, pp. 17693–17703.

[29] S. Yang, D. Zhou, J. Cao, and Y. Guo, "LightingNet: An integrated learning method for low-light image enhancement," *IEEE Trans. Comput. Imag.*, vol. 9, pp. 29–42, 2023.

[30] A. Dosovitskiy, L. Beyer, A. Kolesnikov, D. Weissenborn, X. Zhai, T. Unterthiner, M. Dehghani, M. Minderer, G. Heigold, S. Gelly, J. Uszkoreit, and N. Houlsby, "An image is worth 16×16 words: Transformers for image recognition at scale," 2020, *arXiv:2010.11929*.

[31] X. Wang, K. Chen, Z. Wang, and W. Huang, "PMSNet: Parallel multi-scale network for accurate low-light light-field image enhancement," *IEEE Trans. Multimedia*, early access, Jul. 3, 2023, doi: 10.1109/TMM.2023.3291498.

[32] R. Mantiuk, S. Daly, and L. Kerofsky, "Display adaptive tone mapping," in *Proc. ACM SIGGRAPH Papers*, Aug. 2008, pp. 1–10.

[33] C. Schlick, "Quantization techniques for visualization of high dynamic range pictures," in *Photorealistic Rendering Techniques*. Berlin, Germany: Springer, 1995, pp. 7–20.

[34] L. Wang and C. Jung, "Surrounding adaptive tone mapping in displayed images under ambient light," in *Proc. IEEE Int. Conf. Acoust., Speech Signal Process. (ICASSP)*, Mar. 2017, pp. 1992–1996.

[35] C. J. Bartleson and E. J. Breneman, "Brightness perception in complex fields," *J. Opt. Soc. Amer.*, vol. 57, no. 7, pp. 953–957, 1967.

[36] H. Su, C. Jung, L. Wang, S. Wang, and Y. Du, "Adaptive tone mapping for display enhancement under ambient light using constrained optimization," *Displays*, vol. 56, pp. 11–22, Jan. 2019.

[37] J. Bauer, *Effiziente Und Optimierte Darstellungen Von Informationen Auf Grafikanzeigen Im Fahrzeug: Situationsadaptive Bildaufbereitungsalgorithmen Und Intelligente Backlightkonzepte*. Karlsruhe, Germany: KIT Scientific, 2013.

[38] K. R. Prabhakar and R. V. Babu, "Ghosting-free multi-exposure image fusion in gradient domain," in *Proc. IEEE Int. Conf. Acoust., Speech Signal Process. (ICASSP)*, Mar. 2016, pp. 1766–1770.

[39] O. Ronneberger, P. Fischer, and T. Brox, "U-Net: Convolutional networks for biomedical image segmentation," in *Proc. Int. Conf. Med. Image Comput. Comput.-Assist. Intervent.* Berlin, Germany: Springer, 2015, pp. 234–241.

[40] Z. Wang, A. C. Bovik, H. R. Sheikh, and E. P. Simoncelli, "Image quality assessment: From error visibility to structural similarity," *IEEE Trans. Image Process.*, vol. 13, no. 4, pp. 600–612, Apr. 2004.

[41] W. Huang, Y. Zhu, and R. Huang, "Low light image enhancement network with attention mechanism and Retinex model," *IEEE Access*, vol. 8, pp. 74306–74314, 2020.

[42] K. Simonyan and A. Zisserman, "Very deep convolutional networks for large-scale image recognition," 2014, *arXiv:1409.1556*.

[43] X. Li, D. Song, and Y. Dong, "Hierarchical feature fusion network for salient object detection," *IEEE Trans. Image Process.*, vol. 29, pp. 9165–9175, 2020.

[44] E. Reinhard, W. Heidrich, P. Debevec, S. Pattanaik, G. Ward, and K. Myszkowski, *High Dynamic Range Imaging: Acquisition, Display, and Image-Based Lighting*. Burlington, MA, USA: Morgan Kaufmann, 2010.

[45] A. Mittal, R. Soundararajan, and A. C. Bovik, "Making a 'completely blind' image quality analyzer," *IEEE Signal Process. Lett.*, vol. 20, no. 3, pp. 209–212, Mar. 2013.

[46] J. Ke, Q. Wang, Y. Wang, P. Milanfar, and F. Yang, "MUSIQ: Multi-scale image quality transformer," in *Proc. IEEE/CVF Int. Conf. Comput. Vis. (ICCV)*, Oct. 2021, pp. 5128–5137.

JUNMIN LEE received the B.S. degree in electronic engineering from Inha University, Incheon, South Korea, in 2021, where she is currently pursuing the M.S. degree in electrical and computer engineering. Her research interests include computer vision and image processing.

HEEJIN LEE received the B.S. degree in information and communication engineering from Inha University, Incheon, South Korea, in 2021, where she is currently pursuing the M.S. degree in electrical and computer engineering. Her research interests include computer vision and machine learning.

SEUNGHYUN LEE (Associate Member, IEEE) received the B.S. degree in electronic engineering from Inha University, Incheon, South Korea, in 2017, where he is currently pursuing the Ph.D. degree in electronic engineering. His research interests include computer vision and machine learning.

JUNHO HEO received the B.S. degree in electronic convergence engineering from Kwangwoon University, Seoul, South Korea, in 2018, and the M.S. degree in electronic engineering from Sogang University, Seoul, in 2020. He joined LX Semicon, Seoul, in 2020. His research interests include computer vision and image processing.

JIWON LEE received the B.S. degree in physics from Sookmyung Women's University, in 1999, and the B.S., M.S., and Ph.D. degrees in electronic engineering from Sogang University, in 2004, 2006, and 2011, respectively. From 2011 to 2019, she was a Senior Engineer with the SIC Center, LGE Electronics Company Ltd., Seoul, South Korea. In 2019, she joined LX Semicon, Seoul, where she is currently the Director. Her research interests include image enhancement, panel compensation, and computer vision in the display industry.

BYUNG CHEOL SONG (Senior Member, IEEE) received the B.S., M.S., and Ph.D. degrees in electrical engineering from the Korea Advanced Institute of Science and Technology, Daejeon, South Korea, in 1994, 1996, and 2001, respectively. From 2001 to 2008, he was a Senior Engineer with the Digital Media Research and Development Center, Samsung Electronics Company Ltd., Suwon, South Korea. In 2008, he joined the Department of Electronic Engineering, Inha University, Incheon, South Korea, where he is currently a Professor. His research interests include the general areas of image processing and computer vision.